ELSEVIER

Composites Science and Technology 60 (2000) 2671–2680

COMPOSITES SCIENCE AND TECHNOLOGY

www.elsevier.com/locate/compscitech

Young's modulus of unidirectional discontinuous-fibre composites☆

Chun-Hway Hsueh *

Metals and Ceramics Division, Oak Ridge National Laboratory, Oak Ridge, TN 37831, USA

Received 5 November 1999; received in revised form 7 March 2000; accepted 6 June 2000

Abstract

Young's modulus of a unidirectional discontinuous-fibre composite is derived in the present study by the use of a modified shear-lag model. To achieve this, correct determination of the stress transfer at the fibre ends and selection of the representative volume element in the analytical model are required. The present predicted stress distribution along the fibre length during uniaxial loading of the composite is in excellent agreement with that obtained from a finite-element analysis. Also, by a judicious choice of the representative volume element for the modified shear-lag model, the predicted Young's modulus of the composite is in excellent agreement with those predicted from the Halpin–Tsai semi-empirical equation, the Eshelby model, and numerical analyses. Comparison is also made with experimental measurements of Young's moduli of aligned particulate- or whisker-reinforced SiC/aluminum-alloy composites, and good agreement is obtained. © 2000 Elsevier Science Ltd. All rights reserved.

Keywords: A. Short-fibre composites; B. Modelling; C. Stress transfer; C. Elastic properties

1. Introduction

Substantial reinforcement can be achieved by incorporating aligned fibres in the matrix with the fibre axis parallel to the loading direction, and there has been a rapid growth in the use of short-fibre composites because of their great versatility, high performance, and ease of fabrication [1–7]. There has been extensive study of the mechanical properties of these composites, and a comprehensive review of predictions of the elastic constants of these composites has been performed recently by Tucker and Liang [8]. Among the elastic constants, the longitudinal Young's modulus is the most fundamental. Theoretical analyses of Young's modulus can be classified into four types: the Halpin–Tsai semi-empirical equation [9], the Eshelby model [10–13], the shear-lag model [13–17], and numerical methods [8,18]. Among the four types of analyses, the shear lag model is considered to be the least accurate one on account of its crude approximation in the analysis [13]. However, among the analytical models, the stress-transfer mechanism between the fibre and the matrix during loading of the composite can only be derived with the shear-lag model. Hence, a question is raised. Can the shear-lag model be improved to allow better prediction of the Young's modulus of the composite?

The purpose of the present study is to improve the prediction of Young's modulus of an aligned short-fibre composite by the shear-lag model and the stress-transfer mechanism. To achieve this, a newly developed modified shear-lag model [19,20] is adopted. First, both the Halpin–Tsai semi-empirical equation and the Eshelby model are summarized. Second, the essence of the modified shear-lag model is presented, and its solutions are then extended to derive the Young's modulus of the composite. Third, the predicted stress-transfer phenomena is compared to the results obtain from a finite-element analysis (FEA) [21]. Fourth, the predicted Young's modulus of the composite is compared to those predicted from the Halpin–Tsai equation and the Eshelby model. Comparison is also made with experimental measurements of the Young's moduli of particulate- or whisker-reinforced SiC/aluminum-alloy composites [22–24]. It is noted that the results derived from the shear-lag model are affected by the selection of the representative volume element (RVE) in modeling,

☆ The submitted manuscript has been authorized by a contractor for the US Government under contract No. DE-ACO596OR2246. According, the US Government retains a nonexclusive, royalty-free license to publish or reproduce the published form of this contribution, or allow others to do so, for US Government purposes.

* Tel.: +1-865-576-6586; fax: +1-865-574-8445.

E-mail address: hsuehc@ornl.gov.

0266-3538/00/$ - see front matter © 2000 Elsevier Science Ltd. All rights reserved.
PII: S0266-3538(00)00128-7

and a simple method is developed in the present study to determine the RVE. Finally, the analytical solutions for the Young's modulus of the composite are compared to those obtained from finite-difference [18] and finite-element [8] analyses.

2. Halpin–Tsai semi-empirical equation and Eshelby model

Both the Halpin–Tsai semi-empirical equation and the Eshelby model can predict the longitudinal Young's modulus of an aligned short-fibre composite quite well, and they are summarized as follows while a more thorough review can be found elsewhere [8,25].

2.1. Halpin–Tsai semi-empirical equation

The Halpin–Tsai semi-empirical equation has been adopted extensively because of its simple formulation. The longitudinal Young's modulus of an aligned short-fibre composite, E_o, can be described by [9]

$$\frac{E_o}{E_m} = \frac{1 + \xi\eta f}{1 - \eta f} \tag{1}$$

where f is the volume fraction of fibres, and η is given by

$$\eta = \frac{(E_f/E_m) - 1}{(E_f/E_m) + \xi} \tag{2}$$

The subscripts, f and m, denote the fibre and the matrix, respectively. The parameter, ξ, is obtained by curve-fitting of the predicted E_o with experimental results, and it represents a measure of the fibre geometry, the packing geometry, and the loading condition. Good agreement between E_o and experimental measurements has been obtained by letting ξ equal twice the aspect ratio of the fibre [9].

2.2. Eshelby model

The Eshelby model was originally derived for the case of loading of an infinite matrix containing an ellipsoidal inclusion [10]. It was then modified by Mori and Tanaka to include the effect of a finite volume fraction of inclusions [11], and has been applied to the case of uniaxial loading of an aligned short-fibre composite [12,26]. Whereas the stress in an ellipsoidal inclusion is uniform on account of the nature of its geometry, the stress in an embedded short fibre is non-uniform. Hence, the Eshelby model cannot be used to predict the stress-transfer phenomenon, which is a local property, in a short-fibre composite. However, in analyzing Young's modulus, which is a global property, of a short-fibre composite, the Eshelby model gives a good approach and it is summarized as follows.

The Cartesian coordinates, X_1, X_2, and X_3, are used, and X_3 is the axis of symmetry of the ellipsoidal inclusion. A stress, σ_o, is applied to the composite in the X_3 direction. In this case, the remote applied strains, ε^a_{ij}, become

$$\varepsilon^a_{11} = \varepsilon^a_{22} = \frac{-\nu_m \sigma_o}{E_m} \tag{3a}$$

$$\varepsilon^a_{33} = \frac{\sigma_o}{E_m} \tag{3b}$$

where ν is Poisson's ratio. In the absence of the inclusion, the deformation throughout the system is uniform; i.e., the applied strain ε^a_{ij}. However, because of the presence of the inclusion, the deformation in the inclusion is perturbed, and the strain due to this perturbation is defined as the constrained strain, ε^c_{ij}. To solve this problem, the true inclusion is replaced by an equivalent inclusion, which has the same elastic constants as the matrix and undergoes an equivalent transformation strain, ε^t_{ij}. However, this replacement is subjected to the requirement that the displacement and the stress within the true and the equivalent inclusions are identical, such that [10]

$$K_e(\varepsilon^c + \varepsilon^a) = K_m\left(\varepsilon^c + \varepsilon^a - \varepsilon^t\right) \tag{4a}$$

$$G_e\left('\varepsilon^c_{ij} +' \varepsilon^a_{ij}\right) = G_m\left('\varepsilon^c_{ij} +' \varepsilon^a_{ij} -' \varepsilon^t_{ij}\right) \tag{4b}$$

where K and G are the bulk modulus and the shear modulus, the subscript, e, denotes the ellipsoidal inclusion, and ε and $'\varepsilon_{ij}$ are the dilatational and the deviatoric strains, respectively.

When the volume fraction of inclusions is finite, the constrained strain in the inclusion consists of two components, such that [11]

$$\varepsilon^c_{ij} = \varepsilon^{c\,\prime}_{ij} + \varepsilon^{c\,\prime\prime}_{ij} \tag{5}$$

where $\varepsilon^{c\,\prime}_{ij}$ is the constrained strain component when a single inclusion is embedded in an infinite matrix, and it can be related to the transformation strain by [10]

$$\varepsilon^{c\,\prime}_{ij} = S_{ijkl}\varepsilon^t_{kl} \tag{6}$$

where S_{ijkl} is the Eshelby tensor and is a function of the aspect ratio of the inclusion and Poisson's ratio of the matrix. The second constrained strain component, $\varepsilon^{c\,\prime\prime}_{ij}$, is introduced to account for the effect of the presence of other inclusions on an inclusion, and can be related to the transformation strain by [11]

$$(1-f)\varepsilon_{ij}^{c''} + f\left(\varepsilon_{ij}^{c} - \varepsilon_{ij}^{t}\right) = 0 \tag{7}$$

The solutions of the strain components, ε_{ij}^{c} and ε_{ij}^{t}, can be obtained by solving Eqs. (3)–(7).

The stress in the ellipsoidal inclusion in the loading direction, σ_e, can be derived from the stress/strain relationship, such that [10]

$$\sigma_e = \frac{\nu_e E_e(\varepsilon^c + \varepsilon^a)}{(1+\nu_e)(1-2\nu_e)} + \frac{E_e\left(\varepsilon_{33}^{c} + \varepsilon_{33}^{a}\right)}{1+\nu_e} \tag{8}$$

The effective Young's modulus of the composite along the loading direction, E_o, can be obtained by dividing the applied stress with the average strain in the composite in the loading direction, such that [27]

$$E_o = \frac{\sigma_o}{\varepsilon_{33}^{a} + f\varepsilon_{33}^{t}} \tag{9}$$

It is noted that formulations of the solutions of ε_{ij}^{c} and ε_{ij}^{t} (and hence σ_e and E_o) are lengthy and have been obtained by Tandon and Weng [12]. Only the results are presented in the present study.

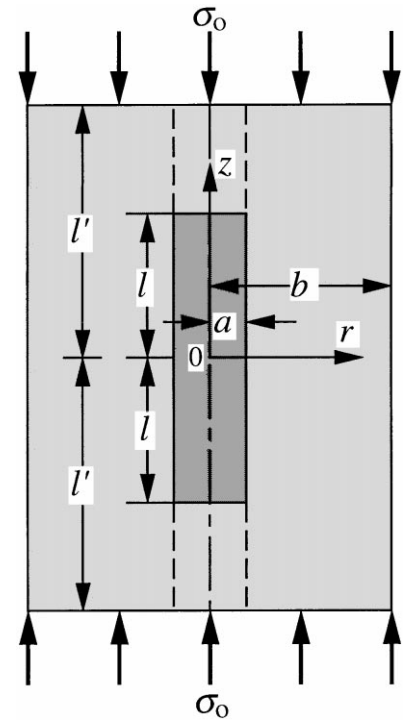

Fig. 1. A schematic showing the representative volume element in the shear-lag model for aligned short-fibre composites. The imaginary fibres are added to analyze the stress transfer at the bonded fibre ends.

3. The modified shear-lag model

The RVE adopted in the shear-lag model is shown in Fig. 1. A discontinuous fibre with a radius a and a length $2l$ is embedded at the centre of a coaxial cylindrical matrix with a radius b and a length $2l'$, such that a^2l/b^2l' corresponds to the volume fraction of fibres in the composite, f.[1] The cylindrical coordinates, r, θ, and z, are used. A tensile stress, σ_o, is applied to the RVE in the z direction. The fibre is bonded to the matrix at both the interface (i.e. at $r = a$) and the ends (i.e., at $z = \pm 1$). The stress is transferred from the matrix to the fibre through both the interface and the fibre ends. The geometry in Fig. 1 is symmetric, and only the region $z \geqslant 0$ needs to be considered.

In the classical shear-lag model [14], the fibre is assumed to sustain only the axial load, the matrix is assumed to transmit only the shear stress, and no load is transferred through the fibre ends (i.e. the fibre ends are debonded from the matrix). It is noted that, in the case of an embedded fibre with bonded fibre ends, the stress at the bonded ends has a finite value, and this stress is required as a boundary condition in order to derive the stress distribution in the fibre. However, this finite stress is not a predetermined value, which, in turn, results in difficulties in using the classical shear-lag model. Various assumptions of this finite stress have been made to solve the stress-transfer problem [16,17].

In the modified shear-lag model [19,20], the radial dependence of the axial stress in the matrix is included in the analysis, the axial-stress distribution in the RVE is in equilibrium with the applied load, the shear-stress distribution in the matrix satisfies the free surface condition at $r = b$, and the boundary condition at the bonded fibre ends is defined by the continuity condition at $z = \pm l$. In order to satisfy this continuity condition, a technique of adding imaginary fibres to the shear-lag model has been developed [19,20]. The matrix connecting the fibre ends to the surface of the RVE (see the area between the dash lines in Fig. 1) is treated as two imaginary fibres, which have the matrix properties. Hence, the stress-transfer problem depicted by Fig. 1 can be solved using two shear-lag models: one for $0 \leqslant z \leqslant l$ and one for $l \leqslant z \leqslant l'$. Although the stress at the fibre end is unknown, the two shear-lag models are jointed at $z = l$ with the continuity condition, which, in turn, determines the stress at the fibre end. Incidentally, a technique developed earlier by Fukuda and Chou [28] by introducing a partially axial load into the matrix in the classical shear-lag model is found to be similar to the "imaginary fibre" technique. Using the methodology described above, the stress transfer problem has been analyzed previously by also including Poisson's effect and residual thermal stresses [20]. The predicted stress

[1] In the classical shear-lag model, the matrix radius, b, is defined by the fibre packing arrangement [8], and the formulation of the fibre volume fraction is different from that defined in the present study.

distribution along the fibre length is in a good agreement with the fluorescence spectroscopy measurement performed on a soda-lime-silicate (SLS) glass matrix containing a single embedded PRD-166 alumina/zirconia fibre subjected to thermo-mechanical loading [20]. It is noted that whereas Poisson's effect is important when the interface at $r = a$ is debonded and frictional [29], it can be ignored when the interface is bonded, in analyzing the stress-transfer problem [30]. Also, the primary interest in the present study is Young's modulus of the composite. Hence, in order to simplify the equations, both Poisson's effect and residual thermal stress are removed from the analysis in Ref. [20], and the axial-stress distributions in the fibre and the imaginary fibre, σ and σ_f', become:

$$\sigma_f = \frac{b^2 E_f \sigma_o}{a^2 E_f + (b^2 - a^2) E_m} + A[\exp(\alpha z) + \exp(-\alpha z)] \quad (\text{for } 0 \leqslant z \leqslant l) \tag{10a}$$

$$\sigma_f{}' = \sigma_o + A'\{\exp(\alpha' z) - \exp[\alpha'(2l' - z)]\} \quad (\text{for } l \leqslant z \leqslant l') \tag{10b}$$

where

$$\alpha = \frac{1}{a} \times \left\{ \frac{a^2 + (b^2 - a^2)\dfrac{E_m}{E_f}}{b^2\left[\dfrac{b^2}{b^2 - a^2}\ln\left(\dfrac{b}{a}\right) - \dfrac{3b^2 - a^2}{4b^2}\right](1 + \nu_m)} \right\}^{1/2} \tag{11a}$$

$$\alpha' = \frac{1}{a}\left\{ \frac{1}{\left[\dfrac{b^2}{b^2 - a^2}\ln\left(\dfrac{b}{a}\right) - \dfrac{3b^2 - a^2}{4b^2}\right](1 + \nu_m)} \right\}^{1/2} \tag{11b}$$

$$A = \frac{(b^2 - a^2)(E_m - E_f)\sigma_o}{a^2 E_f + (b^2 - a^2) E_m} \times \left\{ \exp(\alpha l) + \exp(-\alpha l) - \frac{\alpha[\exp(\alpha l) - \exp(-\alpha l)] \times \{\exp(\alpha' l) - \exp[\alpha'(2l' - l)]\}}{\alpha'\{\exp(\alpha' l) + \exp[\alpha'(2l' - l)]\}} \right\}^{-1} \tag{12a}$$

$$A' = \frac{\alpha[\exp(\alpha l) - \exp(-\alpha l)]A}{\alpha'\{\exp(\alpha' l) + \exp[\alpha'(2l' - l)]\}} \tag{12b}$$

It is noted that although the modified shear-lag model is much more rigorous than the classical shear-lag model, it is not exact and approximations are adopted in deriving the axial stress in the matrix. Also, the axial displacement is non-uniform on the faces of the RVE. In this case, the effective Young's modulus of the RVE in the axial direction is dictated by the average axial displacement at $z = l'$ under the axial loading stress, σ_o. The average axial displacement at $z = l$ is

$$w = \frac{2}{b^2}\left(\int_0^a r \int_0^l \frac{\sigma_f}{E_f}\,dz\,dr + \int_a^b r \int_0^l \frac{\sigma_m}{E_m}\,dz\,dr\right) \tag{13}$$

where σ_m is the axial stress in the matrix. It is noted that whereas the radial dependence of σ_f is ignored in both the classical and the modified shear-lag models as a result of the relatively small fibre radius, the radial dependence of σ_m is considered in the modified shear-lag model [i.e. $\sigma_f(z)$ and $\sigma_m(r, z)$ are considered in the analysis]. However, the explicit expression of σ_m is not required in Eq. (13) in order to solve w. This is because the mechanical equilibrium condition requires

$$2\int_0^a r\sigma_f\,dr + 2\int_a^b r\sigma_m\,dr = b^2\sigma_o \tag{14}$$

The combination of Eqs. (13) and (14) yields

$$w = \frac{l\sigma_o}{E_m} + \frac{a^2}{b^2}\left(\frac{1}{E_f} - \frac{1}{E_m}\right)\int_0^l \sigma_f\,dz \tag{15}$$

Substitution of Eq. (10a) into Eq. (15) gives

$$w = \frac{l\sigma_o}{E_m} + \frac{a^2}{b^2}\left(\frac{1}{E_f} - \frac{1}{E_m}\right) \times \left\{\frac{lb^2 E_f \sigma_o}{a^2 E_f + (b^2 - a^2)E_m} + \frac{A}{\alpha}[\exp(\alpha l) - \exp(-\alpha l)]\right\} \tag{16}$$

Similarly, the average axial displacement at $z = l'$ relative to $z = l$ can be derived from

$$w' = \frac{2}{b^2}\left(\int_0^a r \int_l^{l'} \frac{\sigma_f'}{E_m}\,dz\,dr + \int_a^b r \int_l^{l'} \frac{\sigma_m}{E_m}\,dz\,dr\right) \tag{17}$$

such that

$$w' = \frac{(l' - l)\sigma_o}{E_m} \tag{18}$$

Hence, the average axial displacement at $z = l'$, $w_o(= w + w')$, is

$$w_o = \frac{l'\sigma_o}{E_m} + \frac{a^2}{b^2}\left(\frac{1}{E_f} - \frac{1}{E_m}\right) \times \left\{\frac{lb^2 E_f \sigma_o}{a^2 E_f + (b^2 - a^2)E_m} + \frac{A}{\alpha}[\exp(\alpha l) - \exp(-\alpha l)]\right\} \tag{19}$$

The effective Young's modulus of the RVE in the axial direction, E_o, can be related to the loading stress, the average axial displacement at $z = l'$, and the length of the RVE, such that

$$E_o = \frac{l'\sigma_o}{w_o} \tag{20}$$

A closed-form solution for E_o is hence obtained. However, it is noted that while the elastic constants other than E_o can also be calculated using the Halpin–Tsai equation and the Eshelby model, they cannot be obtained from the shear-lag model.

4. Results

The present predicted stress distribution along the fibre length during uniaxial loading of the composite is compared to that obtained from a FEA. Also, the present analytical solution of longitudinal Young's modulus of an aligned short-fibre composite is compared to the results obtained from the Halpin–Tsai semi-empirical equation, the Eshelby model, experimental measurements, the finite-difference analysis, and the FEA.

4.1. Comparison of stress transfer with finite-element analysis

The stress-transfer problem for the configuration depicted in Fig. 1 has been analyzed using a finite-element analysis, ABAQUS, in which an eight-node, biquadratic axisymmetry solid element is adopted [21]. The material properties used in the FEA are those pertinent to a PRD-166/SLS composite, such that $E_f = 380$ GPa, $E_m = 74$ GPa, $\nu_f = 0.27$, $\nu_m = 0.3$. The dimensions adopted in the FEA are: $b/a = 20$, $l/a = 30$, and $l'/a = 60$, and the solutions of the fibre-axial stress are taken from the fibre elements next to the interface. The results of fibre-axial stress along the loading direction normalized by the loading stress are shown in Fig. 2. The present predicted results of σ_f/σ_o and σ_f'/σ_o are also shown. It is noted that the fibre-axial stress defined in the modified shear-lag model is the average value with respect to the fibre cross-section [19,20] which is different from that defined in the FEA. However, as a result of the small fibre radius, the difference in defining the fibre axial stress between the modified shear-lag model and the FEA is expected to be small. Good agreement between the present analytical results and the FEA results is obtained in Fig. 2. It is also noted that the comparison is based on the solutions obtained from the RVE containing only one fibre. In the case of composites containing multiple fibres, the solutions also depend on the fibre packing arrangement [8].

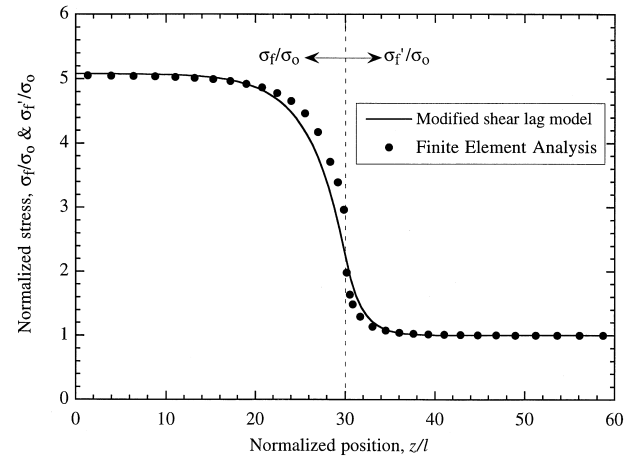

Fig. 2. Comparison of distributions of the normalized axial stress, σ_f/σ_o and $\sigma_{f'}/\sigma_o$, along the axial loading direction between the modified shear-lag model and the finite-element solutions.

4.2. Comparison with the Halpin–Tsai equation, the Eshelby model, and experiments

Aluminum alloys reinforced with SiC particles or whiskers have extensive applications in aircraft engines and aerospace structures. The composite is commonly made by extrusion, and the SiC reinforcement is generally oriented in the extrusion direction. Unless noted otherwise, the material properties of the SiC/Al composite, $E_f = 450$ GPa, $E_m = 72$ GPa, $\nu_f = 0.2$, and $\nu_m = 0.3$, are adopted in the present study to predict Young's modulus of the composite in the extrusion direction. It is noted that with the above material properties, only the aspect ratio and the volume fraction of the reinforcement are needed in using the Halpin–Tsai equation or the Eshelby model to predict the Young's modulus of the composite. However, the specific dimensions of the RVE (i.e. b and l' in Fig. 1) are also required in using the modified shear-lag model because different combinations of b and l' can give the same volume of the RVE. In the literature, two different geometries have been found in choosing a RVE to model a unidirectional discontinuous fibre composite: the RVE scaling with the fibre (i.e. $l'/b = l/a$) [31], and the RVE and the fibre having the same length (i.e. $l' = l$) [13,16,17,32]. It has been noted that $l' = l$ is a good assumption for the case of long embedded fibres and

would induce significant errors for the case of short embedded fibres [13]. The present calculated results using the above two geometries are presented as follows.

To summarize the above two geometries, the radius of the RVE, b, can be related to the fibre radius, a, by

$$b = af^{-p} \tag{21}$$

where $p = 1/3$ when $l'/b = l/a$, and $p = 1/2$ when $l' = l$. Using these two geometries, the predicted effective Young's modulus, E_o, as a function of the fibre-aspect ratio, l/a, is shown in Fig. 3 for $f = 0.2$. The results from the Halpin–Tsai equation and the Eshelby model are also shown. It can be see that the present results are in excellent agreement with the Halpin–Tsai equation for small fibre-aspect ratios ($l/a <\sim 2$) when $l'/b = l/a$ is used, and are in excellent agreement with both the Halpin–Tsai equation and the Eshelby model for large fibre-aspect ratios ($l/a >\sim 10$) when $l' = l$ is used. This trend agrees with the statement that $l' = l$ can only be used for the case of long embedded fibres. Based on the above trend (Fig. 3), a logical selection of the RVE would have p in Eq. (21) increase from 1/3 at small fibre aspect ratios and approach 1/2 as the fibre-aspect ratio increases. A simple equation describing p adopted in the present study is

$$p = \frac{1}{2} - \frac{1}{6}\exp\left(\frac{-l}{5a}\right) \tag{22}$$

The numerical factor in the exponential term in Eq. (22) (i.e. 5) can be varied to adjust how fast p approaches 1/2 as l/a increase. Using Eq. (22), the parameter, p, as a function of the fibre-aspect ratio, l/a, is shown in Fig. 4. Using Eqs. (21) and (22), l' can be obtained by satisfying $a^2 l/b^2 l' = f$, such that

$$l' = lf^{2p-1} \tag{23}$$

Using Eqs. (21)–(23) to define the RVE, the predicted results of E_o for $f = 0.2$ are shown in Fig. 5a, and excellent agreement with both the Halpin–Tsai equation and the Eshelby model is obtained. The results for $f = 0.1$ and 0.3 are shown in Fig. 5b and c, respectively, and excellent agreement is also obtained.

Using $l'/b = l/a$, $l' = l$, and Eq. (23) in the modified shear-lag model, the normalized axial stress distributions, σ_f/σ_o and σ'_f/σ_o, along the axial loading direction are shown in Fig. 6 for $l/a = 3$ and $f = 0.2$. The stress at the loading surface is σ_o (i.e. $\sigma'_f/\sigma_o = 1$ at $z = l'$). When $l' = l$, the stress at the fibre end is the loading stress, σ_o (Fig. 6). The normalized uniform stress in the ellipsoidal inclusion based on the Eshelby model, σ_e/σ_o, is also shown in Fig. 6. While the stress distribution along the fibre length (and hence the stress-transfer phenomena) can be obtained from the modified shear-lag model depending on the RVE selected, the uniform stress in the ellipsoidal inclusion is obtained from the Eshelby model. In the following comparison, Eqs. (21)–(23) are used to define the RVE for the modified shear-lag model.

Experimental measurements of Young's moduli of particulate- or whisker-reinforced SiC/aluminum alloy composites in the extrusion direction, E_o, have been performed. Depending on the composition and the treatment of the aluminum alloy, its Young's modulus can be varied. The material properties of SiC/2124 (T4) [22], SiC/6061 (T6) [23], and SiC/8090 (T6) [24] listed in Table 1 are used for theoretical calculations. The predicted Young's modulus, E_o, based on the modified shear-lag model, the Halpin–Tsai equation, and the Eshelby model are shown in Fig. 7a–c for SiC/2124, SiC/6061, and SiC/8090 composites, respectively. The experimental data [22-24] are also shown, and good

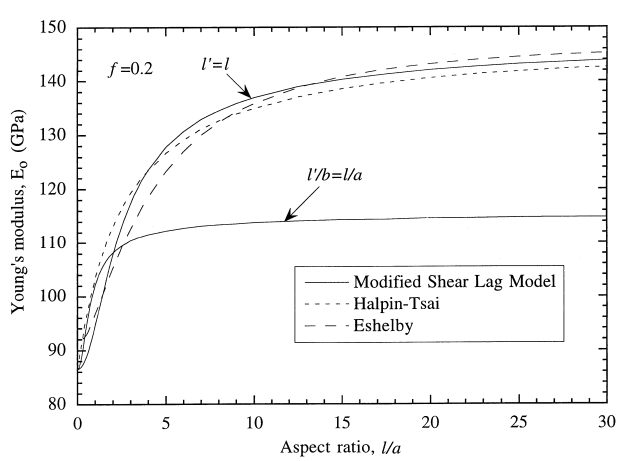

Fig. 3. Longitudinal Young's modulus of SiC/Al composite, E_o, as a function of fibre-aspect ratio, l/a, for $f = 0.2$. The results from the modified shear lag model (assuming $l'/b = l/a$ and $l' = l$), the Halpin–Tsai equation, and the Eshelby model are shown.

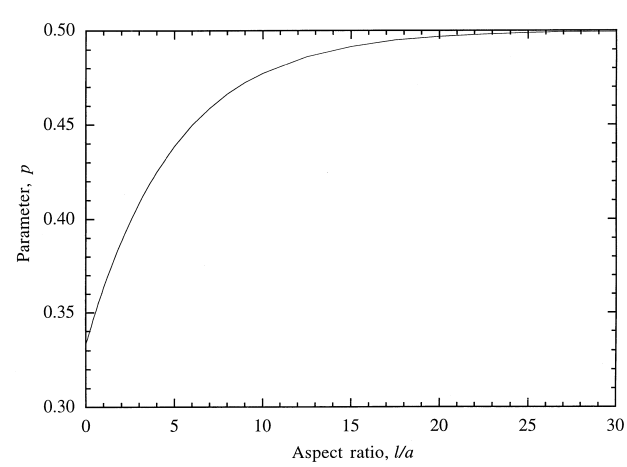

Fig. 4. The parameter, p, in determining the geometry of the representative volume element for aligned short-fibre composites as a function of fibre-aspect ratio, l/a.

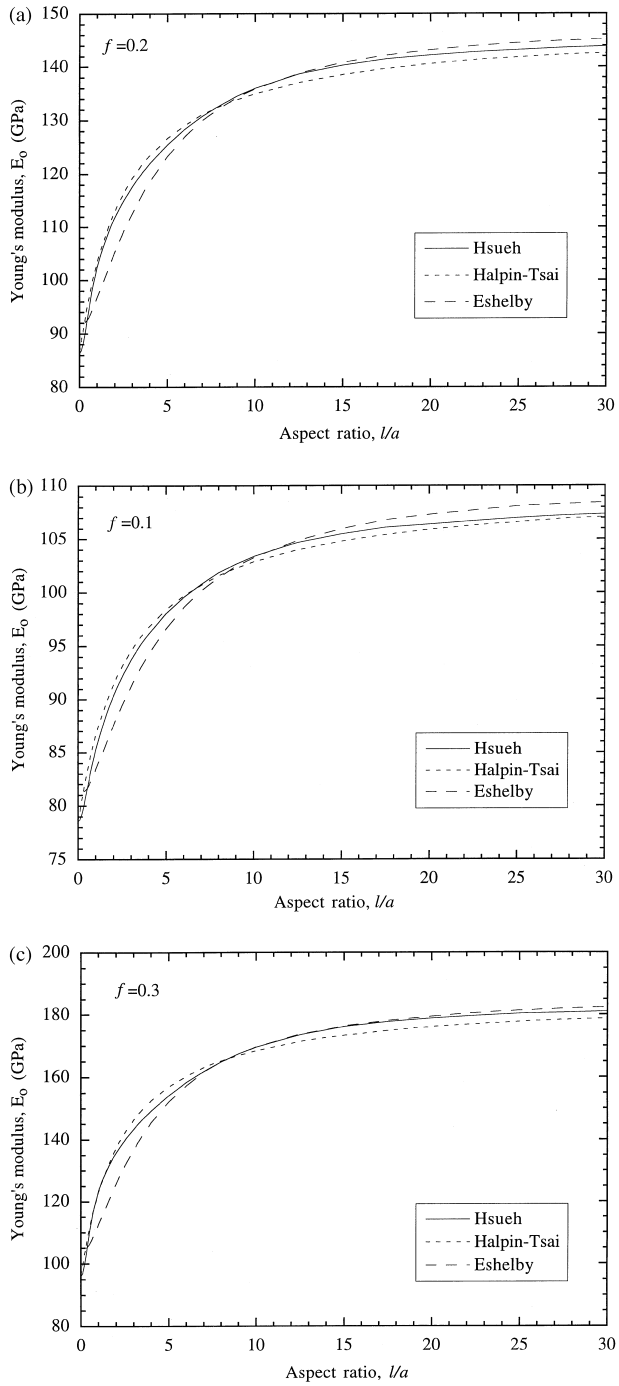

Fig. 5. Longitudinal Young's modulus of SiC/Al composite, E_o, as a function of fibre-aspect ratio, l/a, for (a) $f = 0.2$, (b) $f = 0.1$, and (c) $f = 0.3$. The results from the modified shear-lag model, the Halpin–Tsai equation, and the Eshelby model are shown.

agreement between the three predictions and measurements is obtained.

4.3. Comparison with numerical analyses

Young's modulus of an aligned short-fibre composite has been analyzed numerically using a finite-difference method [18]. However, in order to simplify the analysis, cubic lattices were adopted for both the fibre and the matrix in the finite-difference analysis. Hence, instead of the cylindrical geometry depicted by Fig. 1, the geometry considered in the finite-difference analysis is a rectangular parallelepiped. Also, a multiple-fibre composite was adopted in the finite difference analysis. The difference in geometry between the modified shear-lag model and the finite-difference model would result in differences in the magnitude of the calculated results. However, since Young's modulus of the composite, E_o, is a global property, the difference in its prediction as a result of different geometries is expected to be small. The mechanical properties used in the finite-difference analysis are: $E_f/E_m = 20$ and $\nu_f = \nu_m = 0.3$, and the results were calculated for $l/a = 2$ and 10, respectively, at different fibre-volume fractions. The finite-difference results of E_o/E_m as a function of the fibre-volume fraction, f, are shown in Fig. 8. The predictions based on the modified shear-lag model, the Halpin–Tsai equation, and the Eshelby model are also shown, and good agreement is obtained. It is noted that the results from the modified shear lag model almost overlap with those

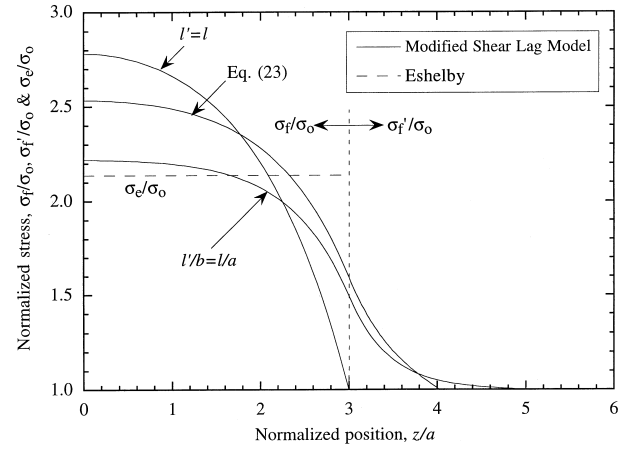

Fig. 6. The normalized axial stress distributions, σ_f/σ_o and $\sigma_{f'}/\sigma_o$, from the modified shear lag model using $l'/b = l/a$, $l' = l$, and Eq. (22), and the uniform normalized stress, σ_e/σ_o, in the ellipsoidal inclusion in the loading direction based on the Eshelby model. The results are shown for SiC/Al composites with $l/a = 3$ and $f = 0.2$.

Table 1
Properties of particulate- or whisker-reinforced SiC/aluminum alloy composites

Composite	Reinforcement	E_e or E_f (GPa)	E_m (GPa)	ν_e	ν_m	Aspect ratio, l/a
SiC/2124 (T4)[a]	Particulate	450	72	0.2	0.3	1.6
SiC/6061 (T6)[a]	Particulate	450	71.7	0.2	0.3	3
SiC/8090 (T6)	Whisker	480	78.2	0.2	0.3	4

[a] T4; room temperature aged; T6; heat treated.

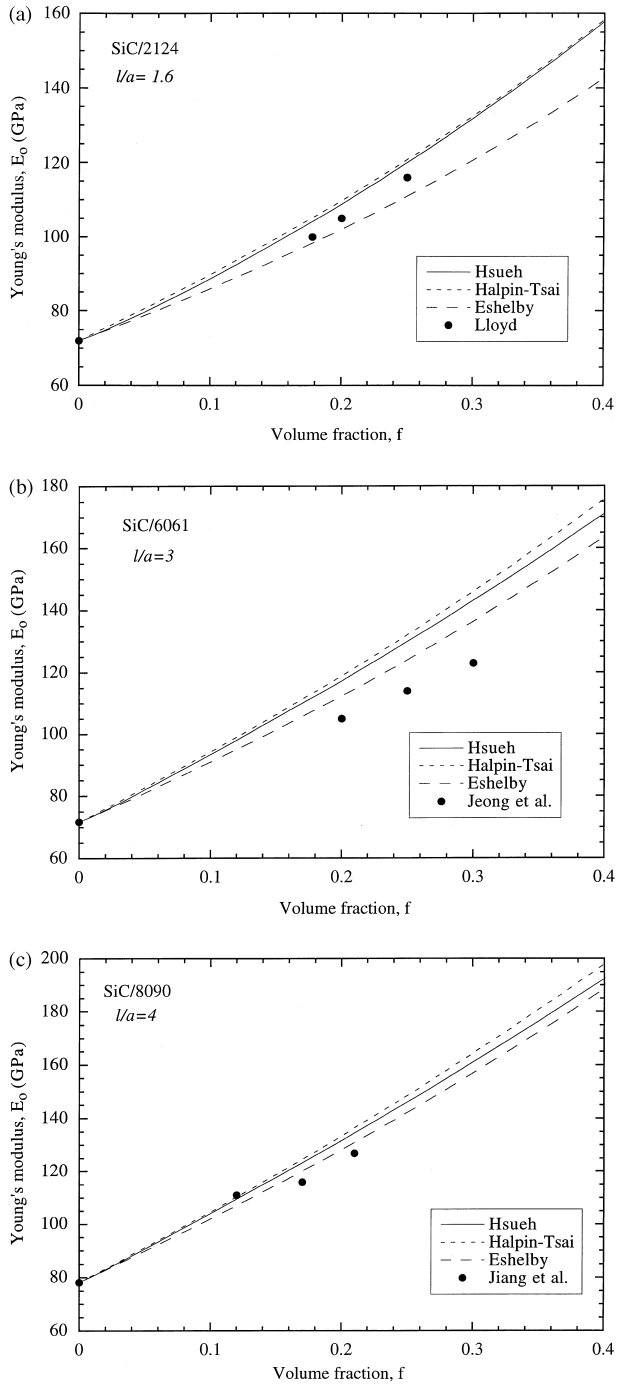

Fig. 7. Longitudinal Young's modulus, E_o, as a function of fibre-volume fraction, f, for (a) SiC/2124, (b) SiC/6061, and (c) SiC/8090 composites. The results from the modified shear lag model, the Halpin–Tsai equation, the Eshelby model, and experimental measurements are shown.

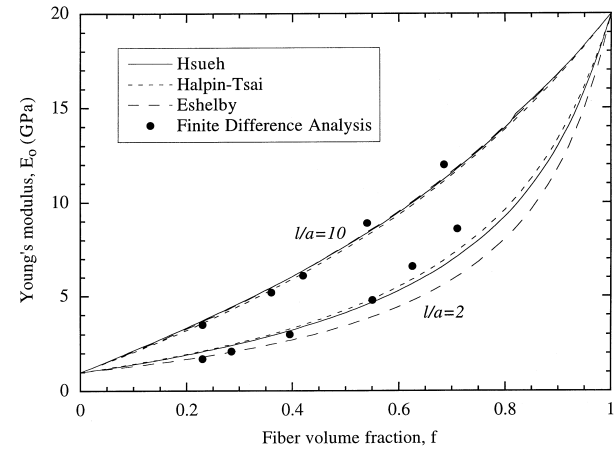

Fig. 8. Longitudinal Young's modulus of aligned short-fibre composites, E_o, as a function of fibre-volume fraction, f, for $l/a = 2$ and 10. The results from the modified shear-lag model, the Halpin–Tsai equation, the Eshelby model, and the finite-difference analysis are shown.

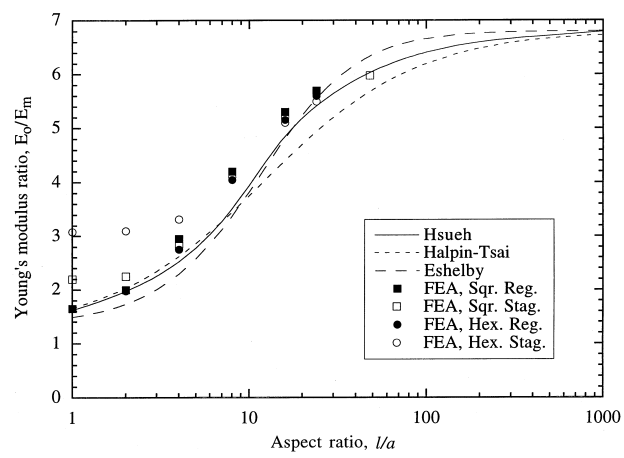

Fig. 9. Normalized longitudinal Young's modulus of aligned short fibre composites, E_o/E_m, as a function of fibre aspect ratio, l/a, for $f = 0.2$. The results from the modified shear-lag model, the Halpin–Tsai equation, the Eshelby model, and the finite-element analysis are shown.

from Eshelby model when $l/a = 10$, and they can hardly be distinguished in Fig. 8.

Young's modulus of an aligned short-fibre composite has also been analyzed using a FEA [8]. Two types of fibre packing arrangements and two types of periodic, three-dimensional arrays of fibres are considered in defining the RVE for the FEA which, in turn, result in four different geometries for the RVE. The two fibre packing arrangements are square and hexagonal, and the two fibre arrays are regular and stagger [8]. The material properties used in the FEA are those pertinent to fibre-reinforced engineering thermoplastics, such that $E_f/E_m = 30$, $\nu_f = 0.2$, $\nu_m = 0.38$. The volume fraction of fibres adopted is 0.2, and different fibre-aspect ratios are used to calculate the effective Young's modulus, E_o, of the RVE. The calculated results of E_o/E_m as a function of the fibre-aspect ratio, l/a, are shown in Fig. 9. The different fibre packing/arrays create scatter in the finite element results. The scatter is small for $l/a \geqslant 8$, but it is significant for $l/a \leqslant 4$. It is believed that the lower finite-element values are more representative of the actual packing and the actual stiffness of composites with very short fibres [8]. The predictions based on the modified shear-lag model, the Halpin–Tsai equation, and the

Eshelby model are also shown in Fig. 9, and good agreement is obtained between the predictions and the lower finite-element values.

5. Conclusions

The Young's modulus of an aligned short-fibre composite is of interest. The theoretical prediction of this value from a shear-lag model is known to be less accurate than those predicted from the Halpin–Tsai semi-empirical equation and the Eshelby model. This is a result of the crude approximation adopted in the shear-lag model. It is noted that the shear-lag model was originally developed to address the stress-transfer problem between the fibre and the matrix. However, whereas the Halpin–Tsai equation and the Eshelby model offer a good prediction of the Young's modulus, they cannot be used to analyze the stress transfer problem for an aligned short-fibre composite. The present study aims at improving the shear-lag model to give better predictions of both Young's modulus and the stress-transfer phenomena in the composite. To achieve this, a rigorous modified shear-lag model is required. This modified shear-lag model has been developed [19,20], and it is then used in the present study to derive the Young's modulus of the composite. However, an inherent problem in the shear-lag model remains in the modified shear lag model; i.e. a representative volume element (RVE) is required in modelling. To resolve this problem, a simple criterion for selecting the RVE is established in the present study [see Eqs. (21)–(23)]. The present predicted stress distribution along the fibre length during uniaxial loading of the composite (Fig. 1) is compared to that obtained from a finite-element analysis, and excellent agreement is obtained (Fig. 2). Also, by a judicious choice of the representative volume element for the modified shear-lag model, the predicted Young's modulus of the composite is in excellent agreement with those predicted from the Halpin–Tsai semi-empirical equation, the Eshelby model, and the numerical analyses (Figs. 5, 8, and 9). Comparison is also made with experimental measurements of Young's moduli of particulate- or whisker-reinforced SiC/aluminum alloy composites, and good agreement is obtained (Fig. 7a–c).

Acknowledgements

The author is grateful to Professor N.A. Yu for making the finite element data in Ms. Y. Zhang's Master Thesis available, and thanks Drs. P.F. Becher, K. Breder, and M.J. Lance for reviewing the manuscript. Research sponsored by US Department of Energy, Division of Materials Sciences, Office of Basic Energy Sciences, under contract DE-AC05-96OR22464 with Lockheed Martin Energy Research Corp.

References

[1] Chou TW, Kelly A. Fibre composites. Mat Sci Eng 1976;25:35–40.
[2] Kelly A. Composites in context. Compos Sci Technol 1985;23:171–99.
[3] Mai YW. In: Shah SP, editor. Applications of fracture mechanics to cementitious composites. Netherlands: Martinus Nijhoff Publ., 1985. p. 399–429.
[4] Arsenault RJ. The strengthening of aluminum alloy by fiber and platelet silicon carbide. Mater Sci Eng 6061;1984:64171-181.
[5] McDanels DL. Analysis of stress-strain, fracture, and ductility behavior of aluminum matrix composites containing discontinuous silicon carbide reinforcement. Metall Trans 1985;16A:1105–15.
[6] Becher PF, Hsueh CH, Angelini P, Tiegs TN. Toughening behavior in whisker-reinforced ceramic composites. J Am Ceram Soc 1988;71:1050–61.
[7] Styles CM, Pitcher PD. Forging behavior and properties of metal matrix composites based on mechanically alloyed Al–Mg–Li alloy. Mater Sci Technol 1998;14:913–9.
[8] Tucker CL, Liang E. Stiffness predictions for unidirectional short-fiber composites: review and evaluation. Compos Sci Technol 1999;59:655–71.
[9] Halpin JC. Primer on composite materials: analysis. Lancaster (PA): Technomic, 1984. p. 130
[10] Eshelby JD. The determination of the elastic field of an ellipsoidal inclusion, and related problems. Proc Roy Soc London, A241:376–96
[11] Mori T, Tanaka K. Average stress in matrix and average elastic energy of materials with misfitting inclusions. Acta Metall 1973;21:571–4.
[12] Tandon GP, Weng GJ. The effect of aspect ratio of inclusions on the elastic properties of unidirectionally aligned composites. Polymer Compos 1984;4:327–33.
[13] Taya M, Arsenault RJ. A comparison between a shear lag type model and an Eshelby type model in predicting the mechanical properties of a short fibre composite. Scripta Metall 1987;21(3):349–54.
[14] Cox HL. The elasticity and strength of paper and other fibrous materials. Brit J Appl Phy 1952;3:72–9.
[15] Piggott MR. Load bearing fiber composites. Elmsford (NY): Pergamon Press, 1980. p. 62
[16] Clyne TW. A simple development of the shear lag theory appropriate for composites with a relatively small modulus mismatch. Mater Sci Eng, A122:183–92
[17] Starink MJ, Syngellakis S. Shear lag models for discontinuous composites: fibre end stresses and weak interface layers. Mater Sci Eng, A270:270–7
[18] Termonia Y. Computer model for the elastic properties of short fibre and particulate filled polymers. J Mater Sci 1987;22:1733–6.
[19] Hsueh CH. A modified analysis for stress transfer in fiber-reinforced composites with bonded fibre ends. J Mater Sci 1995;30:219–24.
[20] Hsueh CH, Young RJ, Yang X, Becher PF. Stress transfer in a model composite containing a single embedded fiber. Acta Metall 1997;45(4):1469–76.
[21] Zhang Y. Modeling of stress transfer in fiber-reinforced ceramic matrix composites. Master thesis, Department of Mechanical and Aerospace Engineering and Engineering Science, The University of Tennessee, Knoxville, 1998.

[22] Lloyd DJ. Particle reinforced aluminum and magnesium matrix composites. Inter Mater Rev 1994;39(1):1–23.
[23] Jeong H, Hsu DK, Shannon RE, Liaw PK. Characterization of anisotropic elastic constant of silicon-carbide particulate reinforced aluminum metal matrix composites: part I. Experiment. Metall Mater Trans 1994;25A:799–809.
[24] Jiang Z, Lian J, Yang D, Dong S. An analytical study of the influence of thermal residual stresses on the elastic and yield behaviors of short fiber-reinforced metal matrix composites. Mater Sci Eng 1998;A248:256–75.
[25] Mlekusch B. Thermoelastic properties of short-fibre-reinforced thermoplastics. Compos Sci Technol 1999;59:911–23.
[26] Hsueh CH. Effects of aspect ratios of ellipsoidal inclusions on elastic stress transfer of ceramic composites. J Am Ceram Soc 1989;72:344–7.
[27] Withers PJ, Stobbs WM, Pedersen OB. The application of the Eshelby method of internal stress determination to short fiber metal matrix composites. Acta Metall 1989;37(11):3061–84.
[28] Fukuda H, Chou TW. An advanced shear-lag model applicable to discontinuous fiber composites. J Comp Mater 1981;15:79–91.
[29] Hsueh CH. Some considerations of evaluation of interfacial frictional stress from the indentation technique for fibre-reinforced ceramic composites. J Mater Sci Lett 1989;8:739–42.
[30] Hsueh CH. Some applications of fiber pullout analyses. J Mater Sci Lett 1991;10:29–32.
[31] Levy A, Papazian JM. Tensile properties of short fibre-reinforced SiC/Al composites: part II. Finite-element analysis. Metall Trans 1990;21A:411–20.
[32] Kelly A, Street KN. Creep of discontinuous fibre composites, II. Theory for the steady-state. Proc R Soc Lond 1972;A328:283–93.